ELECTRONIC SUPPLEMENTARY INFORMATION

Tailoring the Structure and Self-Activated Photoluminescence of Carbonated Amorphous Calcium Phosphate Nanoparticles for Bioimaging Applications

Thales R. Machado,[a,*] Carlos E. Zanardo,[a] Raquel R.C. Vilela,[a] Renata R. Miranda,[a] Natália S. Moreno,[a] Celisnolia M. Leite,[a] Elson Longo,[b] and Valtencir Zucolotto[a,*]

[a] GNANO - Nanomedicine and Nanotoxicology Group, Physics Institute of São Carlos, University of São Paulo, 13566-590 São Carlos, SP, Brazil.
[b] CDMF - Center for the Development of Functional Materials, Federal University of São Carlos, 13565-905 São Carlos, SP, Brazil.

*Corresponding author: trmachado@ifsc.usp.br (T.R. Machado)
zuco@ifsc.usp.br (V. Zucolotto)

Table S1. ACP samples prepared by chemical precipitation and initial amounts of the precursors.

Samples	nCa^{2+} (mmol)	nPO_4^{3-} (mmol)	nCO_3^{2-} (mmol)	CO_3^{2-}/PO_4^{3-} molar ratio
ACP1	9	6	-	-
ACP2	9	6	0.375	0.0625
ACP3	9	6	0.75	0.125
ACP4	9	6	1.5	0.25
ACP5	9	6	3	0.5
ACP6	9	6	6	1
ACP7	9	6	12	2
ACP8	9	6	24	4

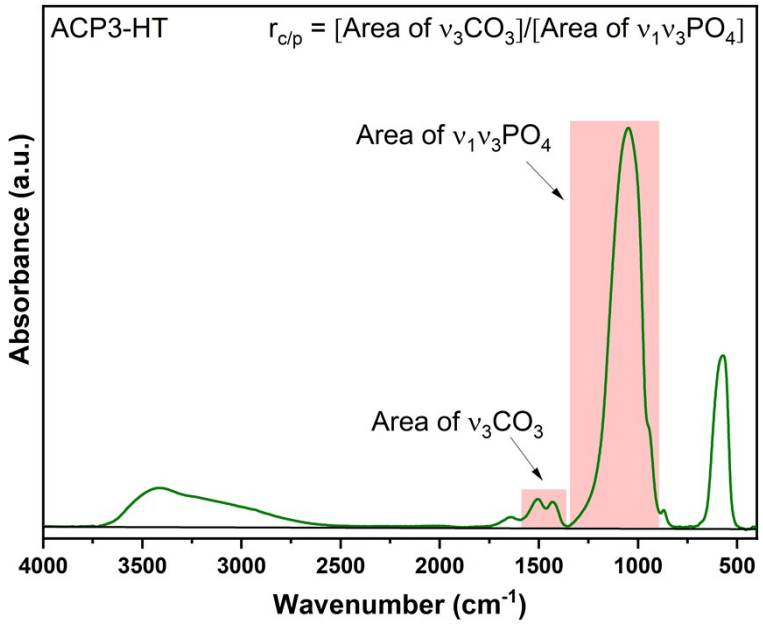

Fig. S1. The carbonate weight percentage ($w(CO_3)$) was determined using the methodology developed by Grunenwald et al. [1], which utilizes FTIR spectroscopy for accurate carbonation analysis in CaP samples including HA and ACP [2,3]. As shown in this figure for ACP3-HT sample, the $w(CO_3)$ was calculated by estimating the ratio $r_{c/p}$ between the integrated areas of the observed ν_3CO_3 bands at ~1590-1350 cm^{-1} and ν_1,ν_3PO_4 bands at ~1300-900 cm^{-1} after conducting a baseline correction and normalization to the ν_3PO_4 mode with the highest absorbance value. Subsequently, the obtained $r_{c/p}$ values were used in the equation $w(CO_3) = 28.62 * r_{c/p} + 0.0843$ to determine the overall degree of carbonation.

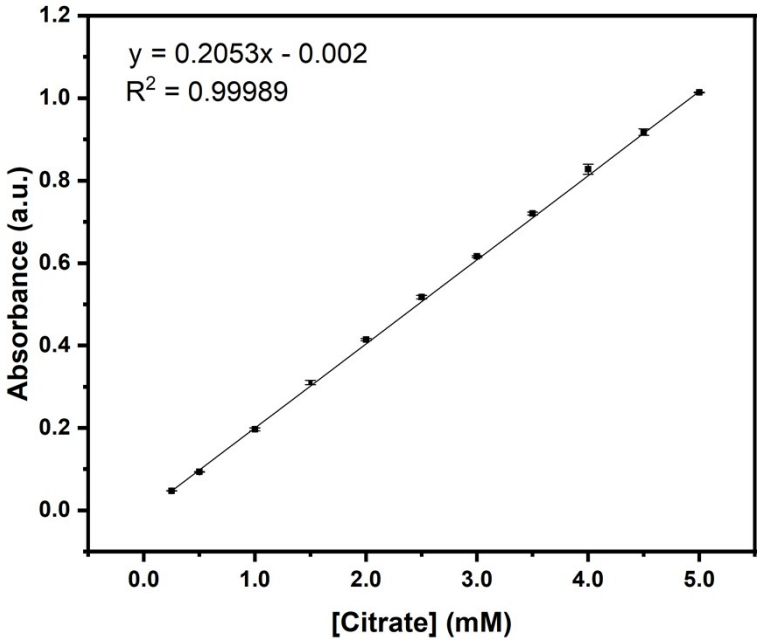

Fig. S2. Standard curve generated from absorbance values at 210 nm, corresponding to the absorption of citrate ions.

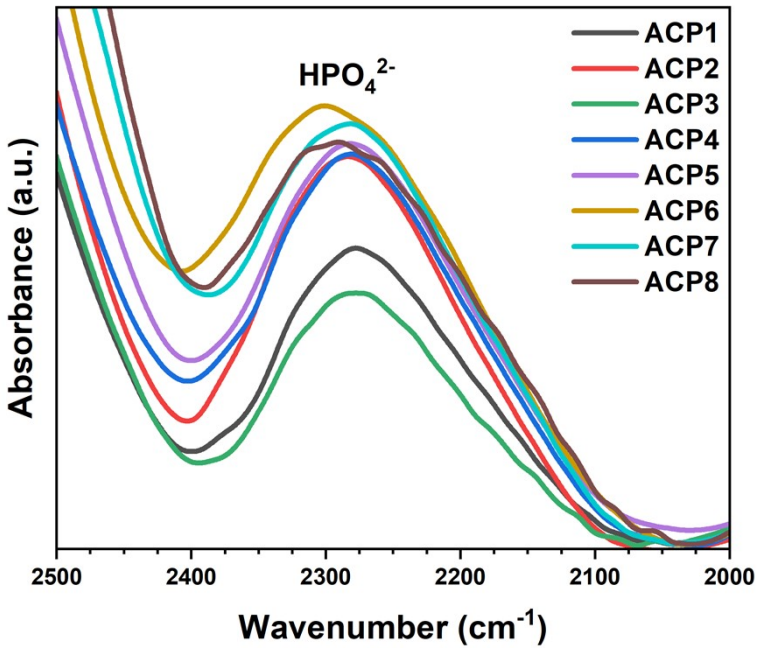

Fig. S3. FTIR spectra evidencing a band between 2500-2100 cm^{-1} attributed to the presence of HPO_4^{2-} in as-synthesized samples [4,5].

Table S2. wCO_3 estimated by elemental analysis of two representative samples.

Sample	wCO_3 (wt.%)
ACP3	2.87
ACP8	27.01

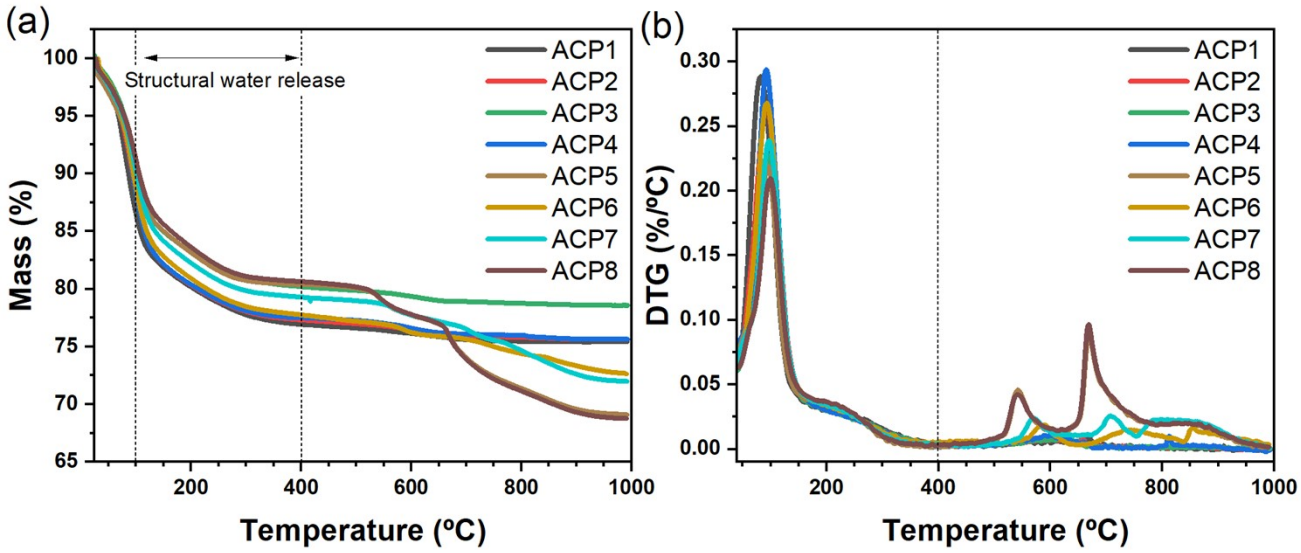

Fig. S4. (a) TGA curves for the as-synthesized ACP NPs, and (b) their corresponding DTG curves.

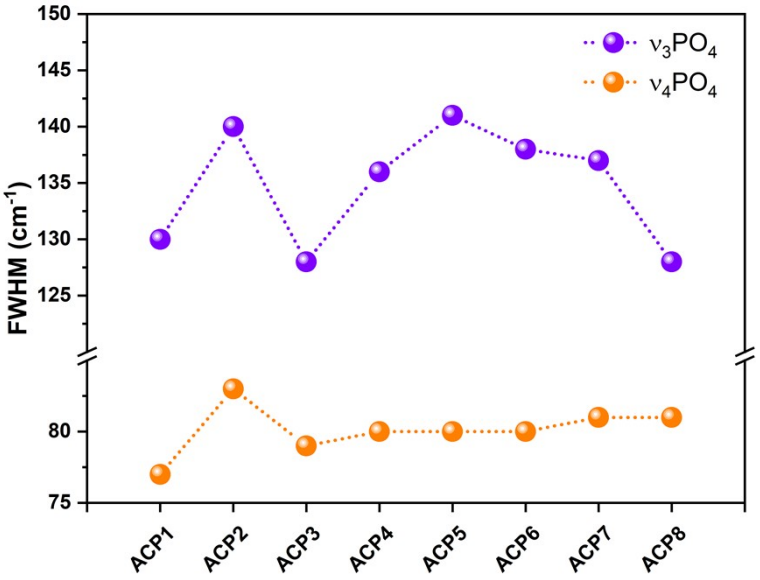

Fig. S5. FWHM of ν_3,ν_4PO_4 bands calculated from the FTIR spectra of as-synthesized samples.

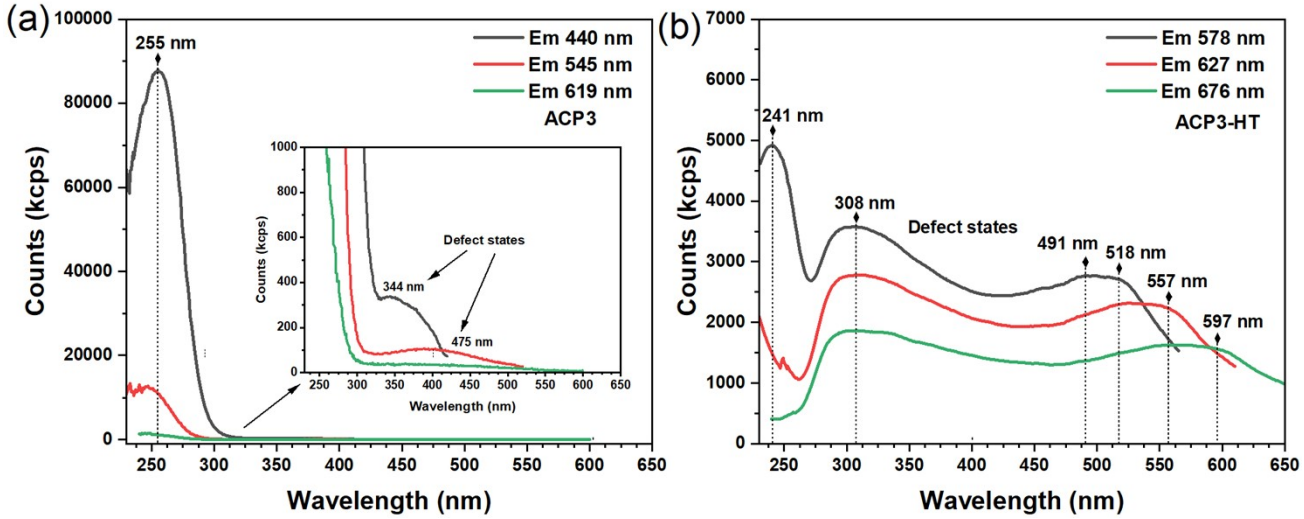

Fig. S6. Excitation spectra for (a) ACP3 NPs and (b) ACP3-HT NPs. The broad and intense bands at 255 nm and 241 nm for ACP3 and ACP3-HT samples, respectively, are attributed to transitions primarily involving band states [5]. The inset in (a) illustrates the defect states contributing to the observed PL emission for ACP3 NPs. Conversely, defect states are predominant in the excitation spectra of ACP3-HT and are distributed across the entire visible spectrum, facilitating the occurrence of PL emission even with low excitation wavelengths.

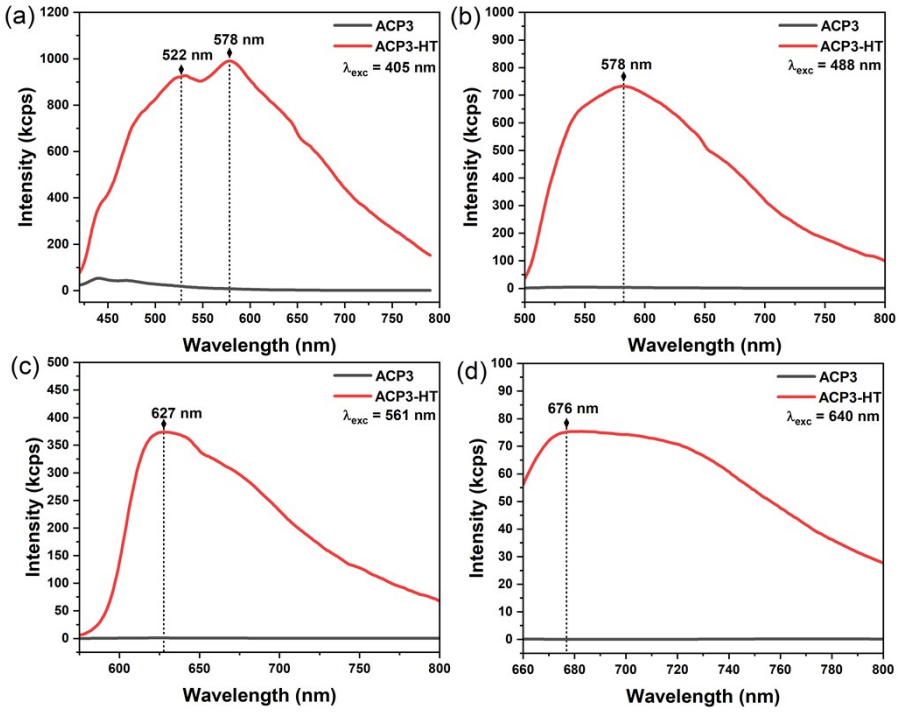

Fig. S7. PL emission spectra of ACP3 and ACP3-HT samples at distinct excitation wavelengths. (a) λ_{exc} = 405 nm, (b) λ_{exc} = 488 nm, (c) λ_{exc} = 561 nm, and (d) λ_{exc} = 640 nm.

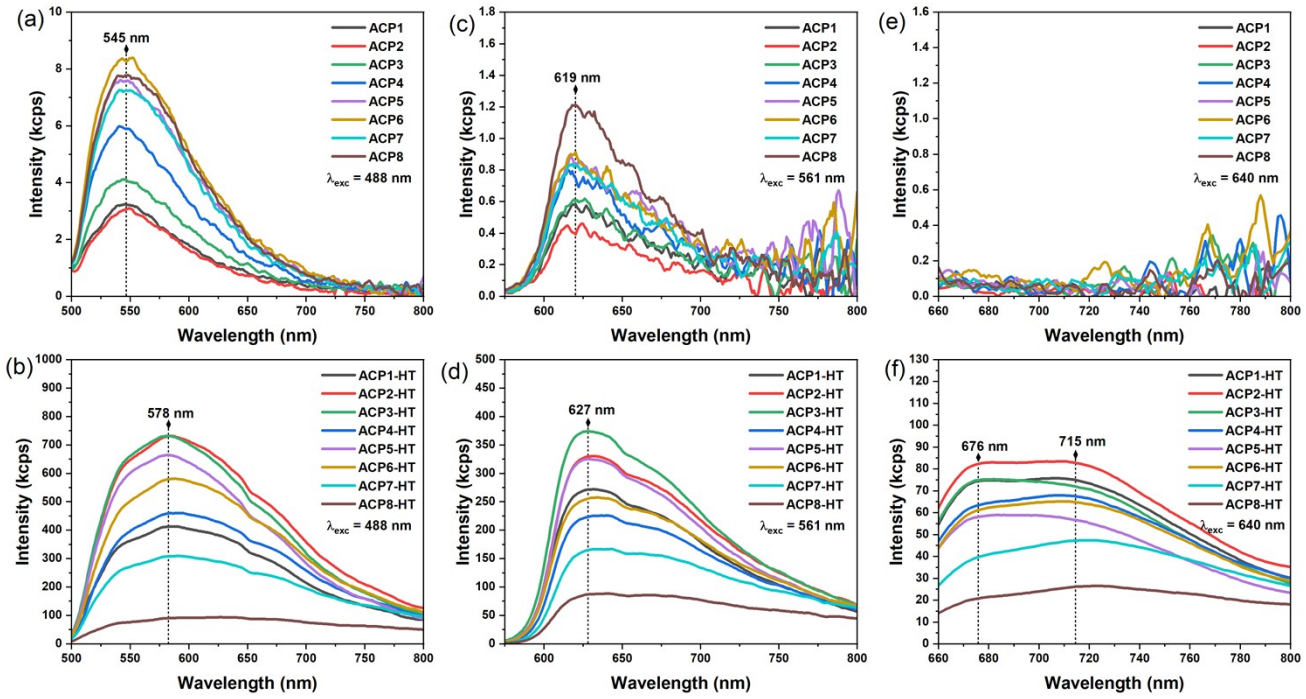

Fig. S8. PL emission spectra of all carbonated ACP NPs samples at distinct excitation wavelengths. (a,b) λ_{exc} = 488 nm, (c,d) λ_{exc} = 561 nm, and (e,f) λ_{exc} = 640 nm.

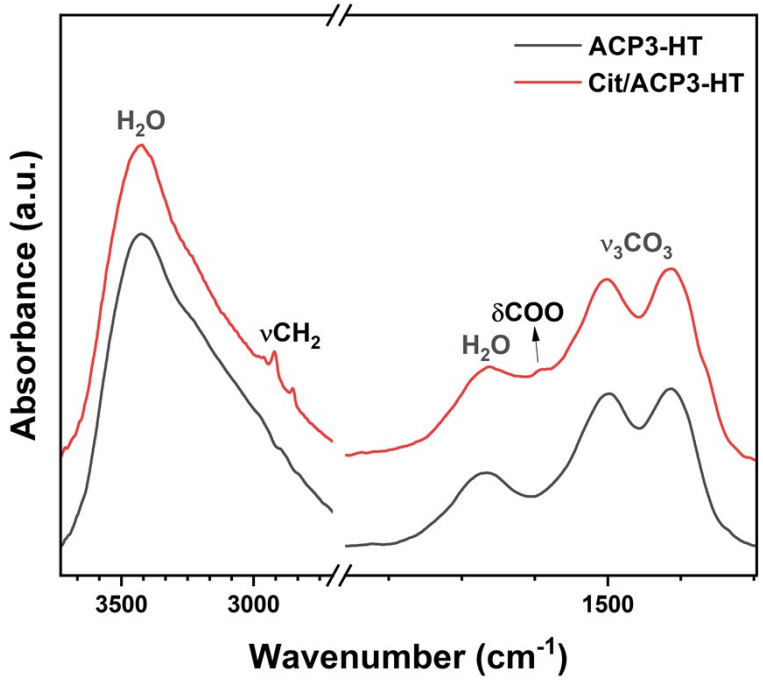

Fig. S9. FTIR spectra of ACP3-HT and Cit/ACP3-HT evidencing the successful functionalization of the NPs with citrate ions.

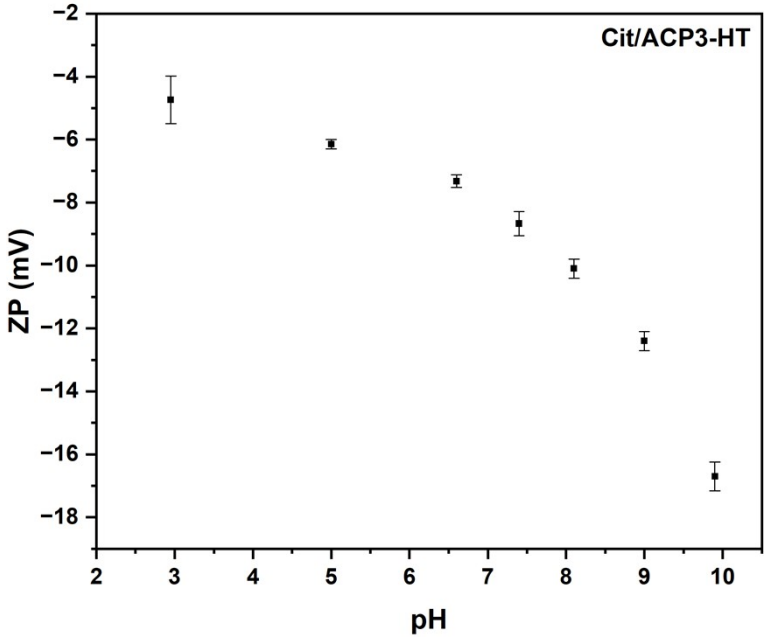

Fig. S10. Zeta potential of Cit/ACP3-HT NPs estimated at various pH values.

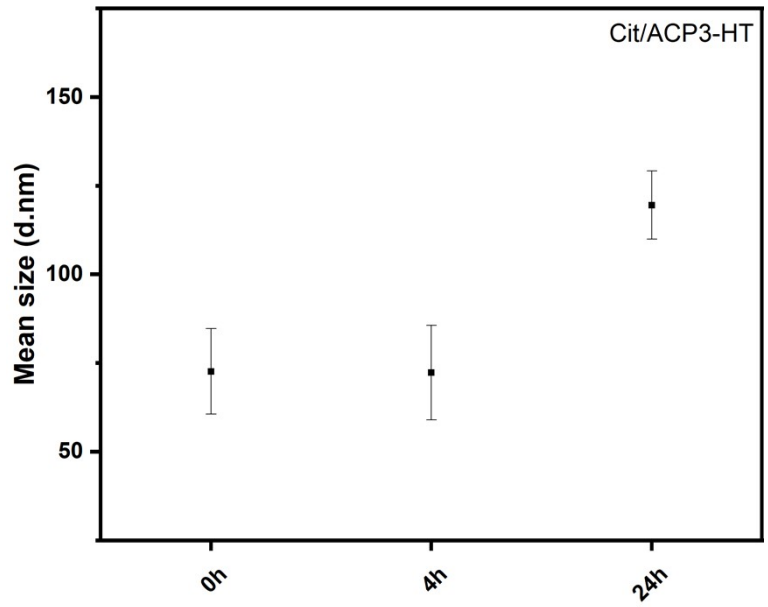

Fig. S11. Mean size of Cit/ACP3-HT NPs measured at different time intervals.

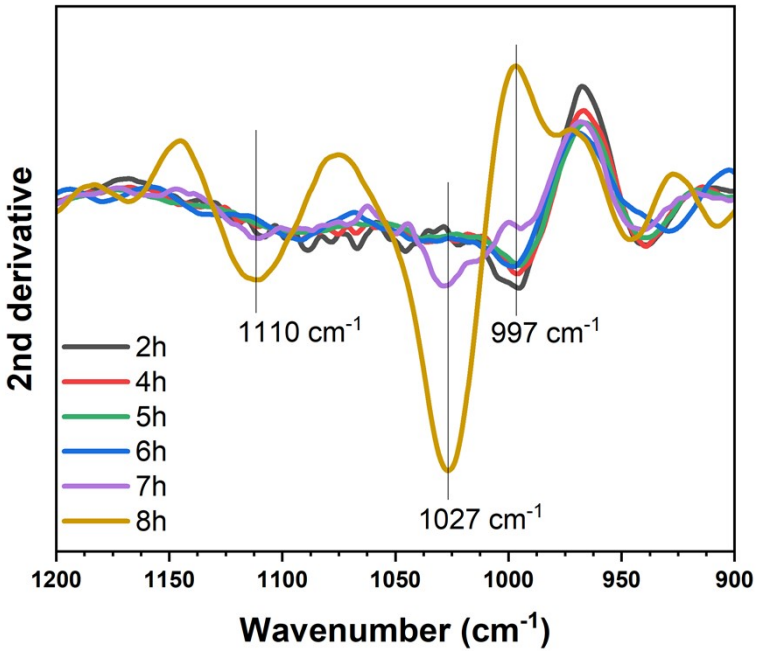

Fig. S12. Second derivate FTIR spectra for ν_3PO_4 modes of ACP3-HT NPs in water.

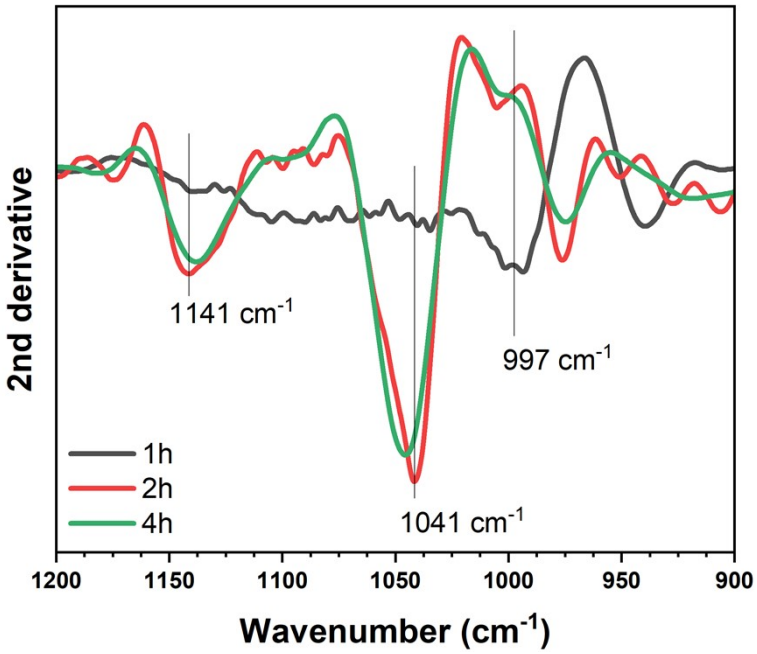

Fig. S13. Second derivate FTIR spectra for ν_3PO_4 modes of Cit/ACP3-HT NPs in PBS (pH 7.4).

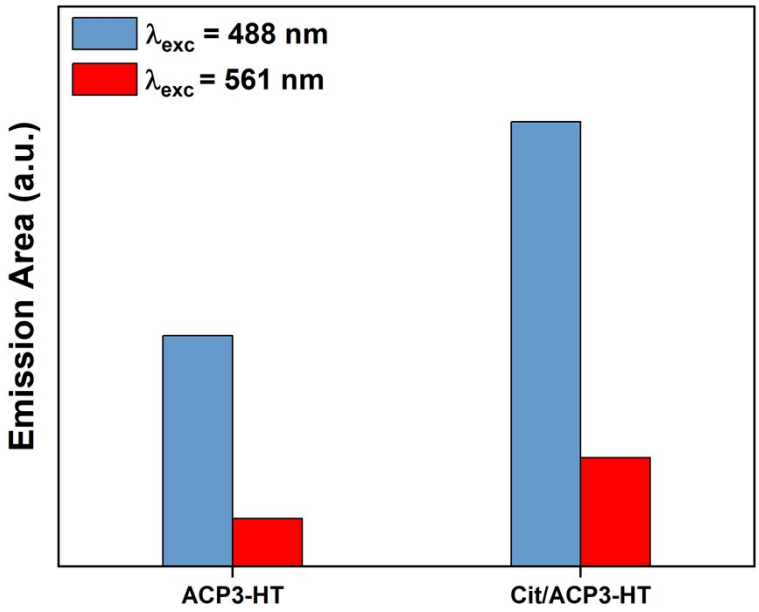

Fig. S14. Integrated emission area of ACP3-HT and Cit/ACP3-HT dispersed at 1mg.mL^{-1} in water.

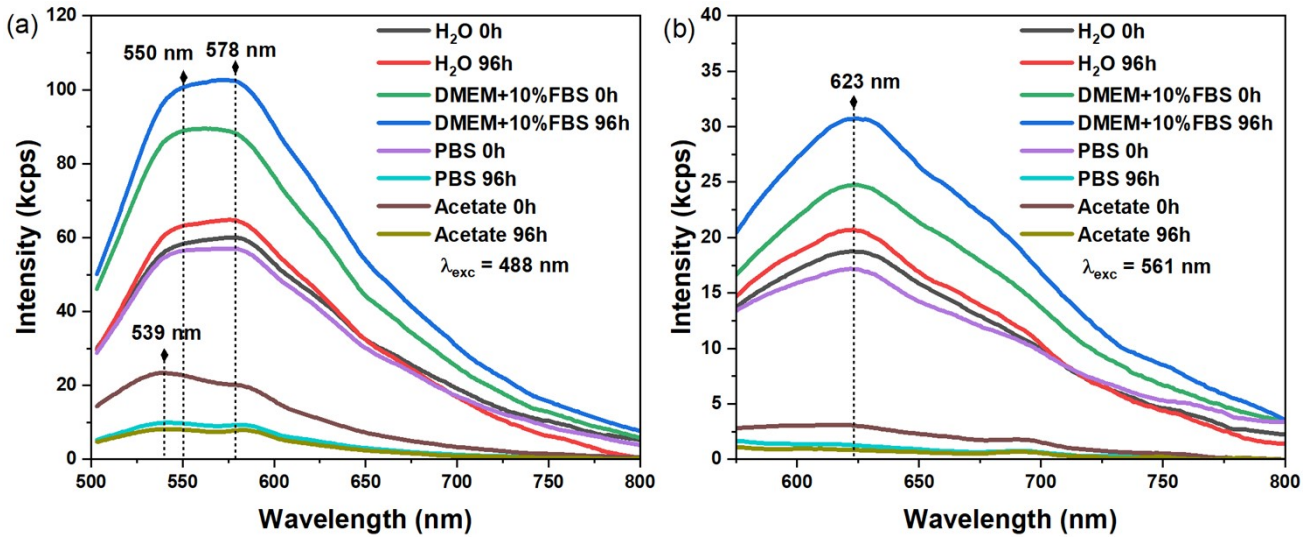

Fig. S15. PL emission spectra of Cit/ACP3-HT NPs in distinct aqueous environments and time intervals, measured at (a) λ_{exc} = 488 nm, and (b) λ_{exc} = 561 nm.

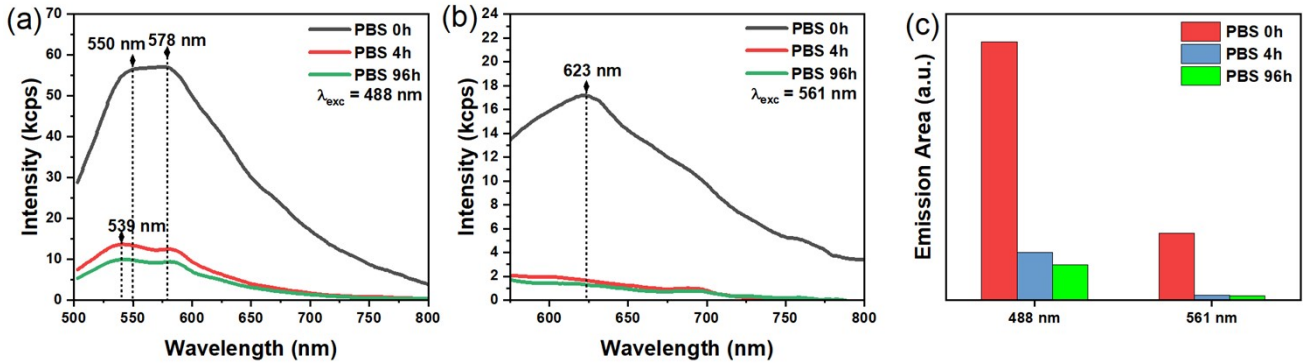

Fig. S16. (a,b) PL emission spectra of Cit/ACP3-HT NPs dispersed at 1 mg.mL^{-1} in PBS (pH 7.4) at distinct time intervals, and (c) their corresponding integrated emission areas.

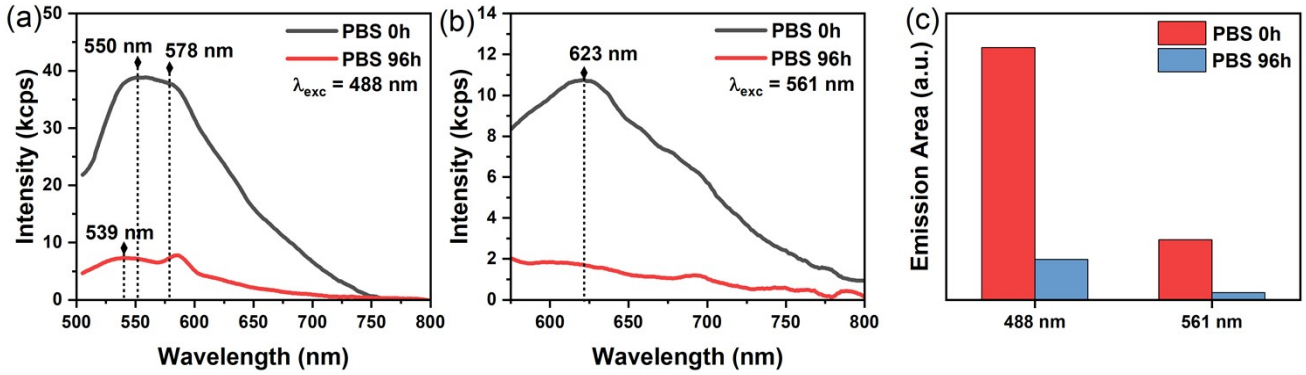

Fig. S17. (a,b) PL emission spectra of ACP3-HT NPs dispersed at 1 mg.mL^{-1} in PBS (pH 7.4) at distinct time intervals, and (c) their corresponding integrated emission areas.

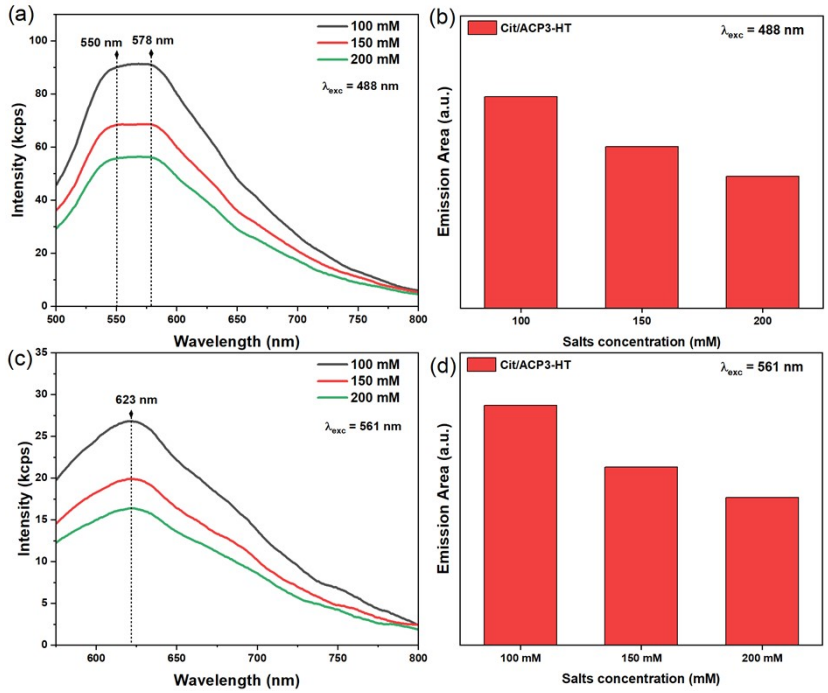

Fig. S18. (a,c) PL emission spectra of Cit/ACP3-HT NPs dispersed at 1 mg.mL^{-1} in Tris-HCl buffer (pH 7.4) at distinct ionic strengths, and (b,d) their corresponding integrated emission areas.

References

[1] A. Grunenwald, C. Keyser, A.M. Sautereau, E. Crubézy, B. Ludes, C. Drouet, Revisiting carbonate quantification in apatite (bio)minerals: A validated FTIR methodology, J Archaeol Sci 49 (2014) 134–141. https://doi.org/10.1016/j.jas.2014.05.004.

[2] M. Luginina, R. Orru, G. Cao, M. Luginina, D. Grossin, F. Brouillet, G. Chevallier, C. Thouron, C. Drouet, First successful stabilization of consolidated amorphous calcium phosphate (ACP) by cold sintering: Toward highly-resorbable reactive bioceramics, J Mater Chem B 8 (2020) 629–635. https://doi.org/10.1039/c9tb02121c.

[3] C. Ortali, I. Julien, C. Drouet, E. Champion, Influence of carbonation on the low-temperature consolidation by Spark Plasma Sintering of carbonated calcium phosphate bioceramics, Ceram Int 46 (2020) 5799–5810. https://doi.org/10.1016/j.ceramint.2019.11.030.

[4] J. Xu, I.S. Butler, D.F.R. Gilson, FT-Raman and high-pressure infrared spectroscopic studies of dicalcium phosphate dihydrate ($CaHPO_4 \cdot 2H_2O$) and anhydrous dicalcium phosphate ($CaHPO_4$), Spectrochimica Acta Part A 55 (1999) 2801–2809.

[5] T.R. Machado, J.S. da Silva, R.R. Miranda, V. Zucolotto, M.S. Li, M.V.M. de Yuso, J.J. Guerrero-González, I.L.V. Rosa, M. Algarra, E. Longo, Amorphous calcium phosphate nanoparticles allow fingerprint detection via self-activated luminescence, Chemical Engineering Journal 443 (2022) 136443. https://doi.org/10.1016/j.cej.2022.136443.